Hyperfine fields at the ^{57}Fe nucleus in monovalent iron ($^6D, 3d^6 4s$) isolated in solid xenon*

P. A. Montano
Department of Physics, West Virginia University, Morgantown, West Virginia 26506

P. H. Barrett and H. Micklitz†
Department of Physics, University of California, Santa Barbara, California 93106

A. J. Freeman
Department of Physics and Astronomy, Northwestern University, Evanston, Illinois 60201

J. V. Mallow
Physics Department, Loyola University of Chicago, Chicago, Illinois 60628

(Received 25 July 1977)

The Mössbauer effect was used to unequivocably identify and measure the effective internal magnetic field at the ^{57}Fe nucleus in monovalent iron in its $^6D, 3d^6 4s$ state isolated in a xenon matrix. The monovalent iron was produced by depositing the iron atoms in a matrix doped with HI and the subsequent electron transfer between the electron donor (Fe^0) and the acceptor species promoted by photoexcitation. For an applied external field of 28 KOe, an induced anisotropic magnetic hyperfine field at the ^{57}Fe nucleus was measured with $H_z = 350 \pm 10$ kOe and $H_x = 700 \pm 10$ kOe. The ground-state Kramers doublet was uniquely determined from the value of *both* the magnetic hyperfine field and the quadrupole splitting, using a crystal-field-theory analysis and results of *ab initio* spin-polarized Hartree-Fock calculations for the $3d^6 4s\ ^1(^6D)$ and $3d^6 4s\ ^1(^4D)$ terms of monovalent iron. The agreement between theory and experiment was found to be excellent. A systematic study of the possible molecular compounds in the Fe-Xe (HI) mixtures was carried out. For high HI concentrations FeI_2 and FeI_3 were observed. For low iron concentrations and 1% HI in xenon only, the monovalent iron ion was observed after photodissociation of HI.

I. INTRODUCTION

Recently reported Mössbauer absorption experiments with rare-gas matrix isolated ^{57}Fe,[1] ^{119}Sn,[2] and[3] ^{125}Te atoms and molecules together with optical absorption experiments on rare-gas matrix isolated atoms[4,5] have shown that the weak binding of the matrix does not change the electronic configuration from that of the free atom or molecule and that only small changes in atomic levels and in the hyperfine interaction occur due to the crystal field produced by the neighboring rare-gas atoms.[4,5] Further, it has been found that under certain conditions, charged species can be generated and trapped within the matrix.[6] Mössbauer studies[7] with ^{57}Fe atoms following the decay of ^{57}Co in solid Xe found two states, $Fe^0(3d^6 4s^2)$ and $Fe^+(3d^7)$, each identified by its respective isomer shift (IS). Micklitz and Litterst[8] reported the Mössbauer spectrum of Fe^+ in the $3d^6 4s^1$ configuration—an ionic state produced by applying Kasai's technique for the production of Cd^+, Cr^+, and Mn^+ in a rare-gas matrix.[6] The process requires the trapping of both electron donor and acceptor species within the matrix, and then promoting an electron transfer between them by photoexcitation. Once the photoexcitation is completed, the return of the electron from the anion to the cation is stopped by the local-potential trap imposed by the electron affinity of the species. Migration of the oppositely charged ions towards each other is prevented by the matrix lattice.

In this paper we report a study of the monovalent iron trapped in a rare-gas matrix. The purpose of our study was to establish in a more definite way, using the nuclear Zeeman effect, whether the spectrum observed can be unequivocably identified as that of the $Fe^+(^6D)$. By applying a large external magnetic field we were able to observe the internal field at the ^{57}Fe nucleus and compare the observed value with that expected from *ab initio* spin-polarized Hartree-Fock calculations for the free-ion species. This method has been successfully applied before to iron monomers in xenon,[9] argon,[10] and nitrogen.[11] To study all the possible molecular compounds in the Fe-Xe (HI) mixture, we carried out a systematic study of the concentration dependence of Fe^+, and identified all the possible molecules that could be observed in the matrix for different iron and HI concentrations. We have also carried out measurements of Fe^+ in Xe (HI) at two different temperatures, so as to determine its effective Debye temperature, which gives a measure of the strength of the bonding between the isolated ion and the matrix.

II. EXPERIMENTAL PROCEDURES

The samples were made in a liquid-helium cryostat, evacuated to a pressure better than 10^{-7} Torr. The iron atomic beam (90% enriched ^{57}Fe) was produced in an alumina crucible contained in a resistance-heated tantalum furnace. The iron atomic beam was co-deposited with a stream of Xe gas containing HI. The Xe and HI mixtures were prepared in a stainless steel container by monitoring their partial pressures. A stream of the mixture was introduced into the cryostat through a needle valve on the side and the sample was deposited at about 4.2 K onto a Be disk mounted within a superconductor magnet. The rare-gas deposition rate was continuously monitored by the attenuation of the 14.4-keV gamma ray of a ^{57}Co-Cu source mounted on the Ta internal shield of the furnace. The iron deposition rate was calculated through the experimentally determined collection efficiency of the Be disk by weighing the crucible before and after a run. Mössbauer spectra was obtained with a conventional constant acceleration spectrometer using a ^{57}Co-Pd source. An enriched ^{57}Fe foil was used for calibration purposes, and the zero velocity is given with respect to this absorber. Kasai's method was used to produce the monovalent state in the matrix.[6] For the uv irradiation of the matrix we used a high-pressure xenon lamp together with a filter combination consisting of uv filter and a solution filter of $NiSO_4 \cdot 6H_2O$ (0.3 g/ml H_2O, 5-cm absorption length). This filter combination is transparent for wavelengths from 2500 to 3100 Å. The samples were irradiated through a quartz window on the side of the cryostat. Micklitz and Litterst[8] proposed that a two-step process takes place during uv irradiation: (i) photodissociation of HI, and (ii) photoexcitation of Fe accompanied by a charge-transfer process between the excited Fe and the I atom. The net reaction can be summarized as

$$Fe + HI \xrightarrow{h\nu} Fe^{+} + I^{-} + H .$$

III. EXPERIMENTAL RESULTS

Several experiments at different iron and HI concentrations were carried out to investigate all the possible molecular compounds that can be formed in the matrix, such as FeI_2, FeI_3, FeI, and FeH, since their presence would, of course, obscure the identification of the monovalent iron.

We observed the formation of iron-iodine compounds by co-deposition of iron with Xe containing 8% HI onto a Be disk at 4.2 K. At the iron concentration used (0.7 at.%), the probability of iron dimer formation is negligible.

In Fig. 1, the Mössbauer spectrum of that sample before uv irradiation shows a single very broad asymmetric line with an IS of -0.75 ± 0.05 mm/sec. Its width (around 2.5 ± 0.1 mm/sec, or three times the normal linewidth observed for the iron monomer in a pure xenon matrix), is probably produced by perturbation of the monomer caused by the neighboring HI. Since there will be different numbers of HI nearest neighbors, a distribution of slightly perturbed monomers is expected, effectively broadening the Mössbauer absorption line.

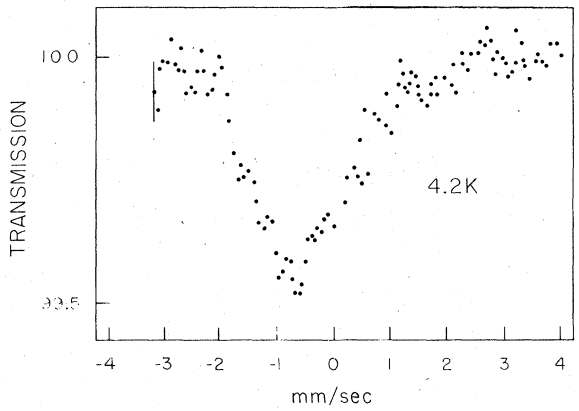

FIG. 1. Mössbauer spectrum of Fe-Xe (8% HI) at 4.2 K.

After the sample was uv irradiated for several hours, a well-defined doublet with a quadrupole splitting (QS) of 1.22 ± 0.02 mm/sec and an IS of 1.06 ± 0.02 mm/sec, was observed (cf. Fig. 2), which is characteristic of divalent compounds. We identified this spectrum with that of the FeI_2 molecule. The IS is slightly more positive than in

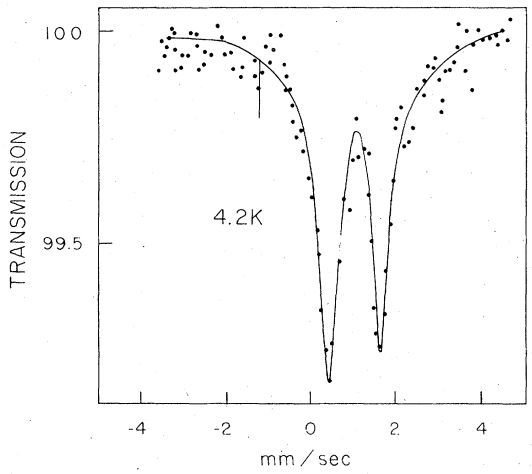

FIG. 2. Mössbauer spectrum of Fe-Xe (8% HI) at 4.2 K after uv irradiation. Solid line is the least-square fit assuming Lorentzian line shape.

the solid, indicating a larger electron density at the nucleus for solid FeI_2. A similar effect was observed in isolated $FeCl_2$ molecules.[12] There is a slight asymmetry in the line in Fig. 2 that might indicate the presence of some FeI_3. We observed that the Mössbauer spectrum of the FeI_2/Xe samples in the presence of an external magnetic field of 28 kOe parallel to the γ-ray direction is characteristic of a compound where the electric field gradient (EFG) axes are randomly distributed. Our fit to the spectrum using the approach of Ref. 13 gives an internal field of 80 ± 10 kOe at the ^{57}Fe nucleus—a value which is very similar to that obtained for amorphous FeI_2.[13]

Upon warming the samples to a temperature of 78 K, the xenon matrix was lost, but residual molecular compounds were left. They are shown in Fig. 3, and can be identified as those of FeI_2 and FeI_3 (FeI_2 at 78 K IS = 1.00 ± 0.02 mm/sec, and QS = 2.13 ± 0.02 mm/sec; FeI_3 at 78 K IS = 0.32 ± 0.02 mm/sec, and QS = 0.87 ± 0.02 mm/sec). Upon warming to room temperature the sample was converted to FeI_2, and the values of the IS and QS agreed with those reported in the literature.

The iron hydrides represent one possible type of molecular compounds that have not been considered in the analysis. Since such molecular compounds do not exist at room temperature in any known stable form, one would expect their formation in the matrix to be hindered by the uv irradiation. However, as the irradiation is strong enough to break the HI bond, an FeH compound could be easily dissociated. It is more likely that the hydrogen will diffuse in the matrix, and be recombined with other hydrogens to form H_2. No

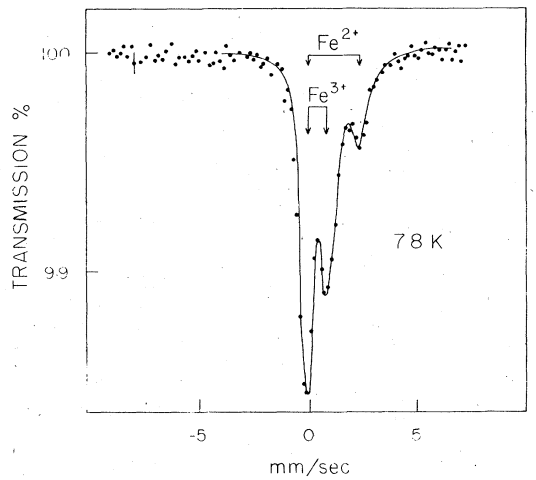

FIG. 3. Mössbauer spectrum of the residual compounds at 78 K of Fe-Xe (8% HI) after uv irradiation. Solid line is the least-square fit assuming Lorentzian line shape.

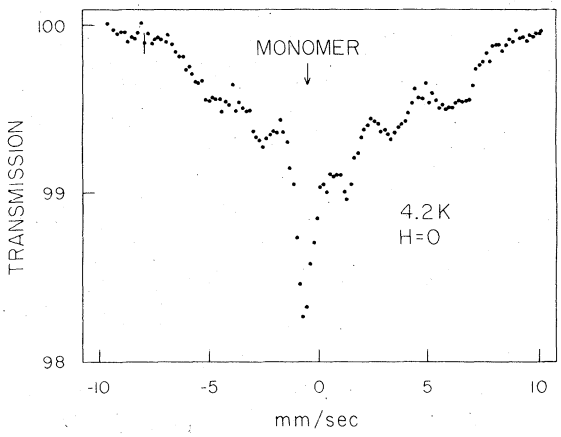

FIG. 4. Mössbauer spectrum of Fe-Xe (1% HI) 2.5 at.% iron at 4.2 K after uv irradiation.

evidence of any well-defined compounds other than FeI_2 and FeI_3 were found in our experiments.

Samples containing an iron concentration greater than 2.5 at.% in a xenon matrix (1% HI) show Mössbauer spectra characterized by the formation of clusters in the matrix. Figure 4 shows a typical example of such a spectrum after 18 h of uv irradiation, the formation of some monovalent iron became detectable, but the resolution of the spectrum is not good enough for a satisfactory analysis. Consequently, it becomes clear that the monovalent iron can only be observed for very restricted concentration ranges of iron and HI in xenon.

A sample was prepared containing 0.9 at.% Fe (200 $\mu g/cm^2$ ^{57}Fe) in a xenon matrix doped with 1% HI. The Mössbauer spectrum before irradiation is shown in Fig. 5. One observes a single-line spectrum with an IS and width characteristic of the iron monomer in a rare-gas matrix: IS = 0.75 ± 0.02 mm/sec, $2\Gamma = 0.80 \pm 0.02$ mm/sec. A

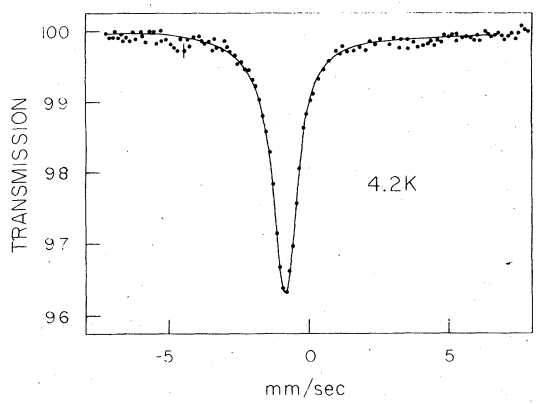

FIG. 5. Mössbauer spectrum of a sample containing 0.9 at.% Fe in xenon (1% HI). The spectrum shows only the monomer line. Solid line is the least-square fit assuming Lorentzian line shape.

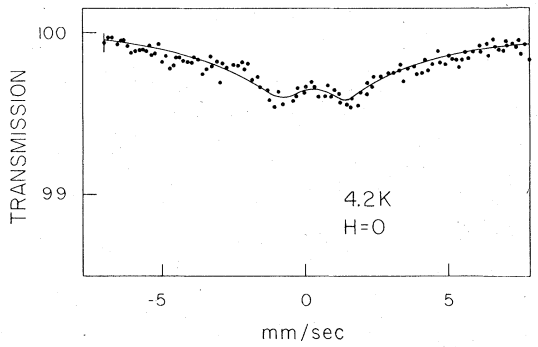

FIG. 6. Mössbauer spectrum of a sample containing 0.9 at.% Fe in xenon (1% HI) at 4.2 after 18 h uv irradiation. The solid line is the fit to the spectrum assuming Lorentzian line shape.

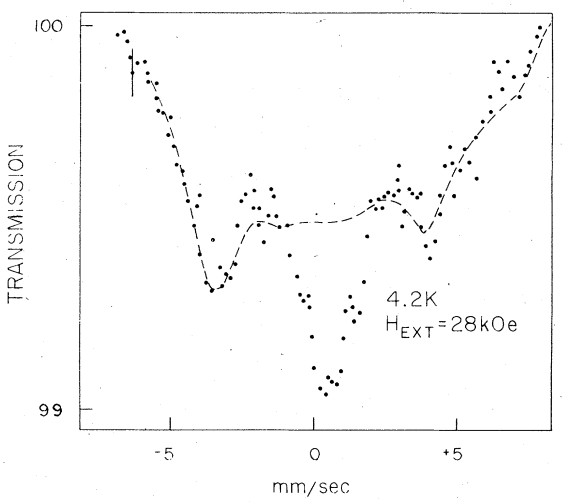

FIG. 7. Mössbauer spectrum of the sample containing 0.9 at.% Fe in xenon (1% HI) at 4.2 K after 18 h uv irradiation in the presence of an external field of 28 kOe. The dashed curve shows a theoretically calculated spectrum with $H_z = 350$ kOe and $H_x = H_y = 700$ kOe.

clean monomer spectrum is obtained with an iron concentration below 1% and HI doping of the xenon of no more than 1%. After uv irradiation of the sample in Fig. 5 for 18 h we observed the spectrum shown in Fig. 6. For this spectrum we measured: IS = 0.29 ± 0.05 mm/sec, QS = 2.1 ± 0.1 mm/sec, and $2\Gamma = 1.8 \pm 0.1$ mm/sec. For this particular concentration selected, about 10% of the original monomer is retained after irradiation. The data was fit using Lorentzian line shapes for three lines and the monomer spectrum was substracted. For smaller iron concentrations the monomer is practically reduced to zero after irradiation (its detection becomes difficult, the effect is less than 0.1%.) However, the resonance effect becomes too small and presents an experimental inconvenience. After irradiation the samples always show the broad doublet seen in Fig. 6. The IS always remains the same within experimental error for different iron concentrations. The QS varies from experiment to experiment depending on the iron and HI concentrations. The reproducibility of the IS as well as its agreement with the expected value for $Fe^+(3d^6 4s)$ suggests that the spectrum was correctly identified as that of monovalent iron.[8] Molecular compounds of iron and iodine show completely different spectra.

We also found an effective Debye temperature for the monovalent iron in the matrix, from the temperature dependence of the Mössbauer spectral area. A value of $\Theta_M = 80 \pm 5$ K is obtained, higher than the one observed for iron monomers in xenon ($\Theta_M = 60$ K), but in good agreement with the Θ_M measured for $Fe^+(3d^7)$ in a xenon matrix (for Fe^+ $Fe^+ 3d^7$, $\Theta_M = 90 \pm 20$ K).[7] The higher value of Θ_M for the monovalent ion can be explained by the polarization of the rare-gas nearest-neighbor atoms that produce a stronger coupling with the matrix.

A measure of the strength of the crystal-field splitting can be obtained from the temperature dependence of the QS. We carried out such measurements for the monovalent iron between 4.2 and 27 K. For the latter temperature we used liquid neon as the cryogenic coolant. The QS at 27 K was 1.7 ± 0.1 mm/sec. Measurements were carried out in the presence of an external magnetic field. The purpose was to measure the internal field at the ^{57}Fe nucleus in monovalent iron and to identify completely the ground-state Kramers doublet. The Mössbauer spectrum for the monovalent iron in the presence of an external magnetic field of 28 kOe collinear with the γ ray is shown in Fig. 7. Mössbauer measurements were carried out at much higher velocities and they failed to reveal any other Mössbauer absorption lines. From the above measurements the ground state was identified as $3d^6 4s\,(^6D)$. The ^4D configuration is too high in energy with respect to the free-ion ground state ^6D.

IV. THEORETICAL INTERPRETATION

A. Quadrupole interaction

The quadrupole splitting of the Mössbauer spectrum in Fig. 6 is produced by EFG at the ^{57}Fe nucleus due mainly to the iodine negative ions. The Fe^+ is surrounded by 12 nearest-neighbor rare-gas atoms that produce a cubic-crystal field at the iron site. The crystal field due to the I^- is superimposed on this field and it is probably stronger than the cubic field. Thus, we can analyze the crystal-field splitting for $Fe^+(^6D)$ using the standard crystal-field approximation. For sim-

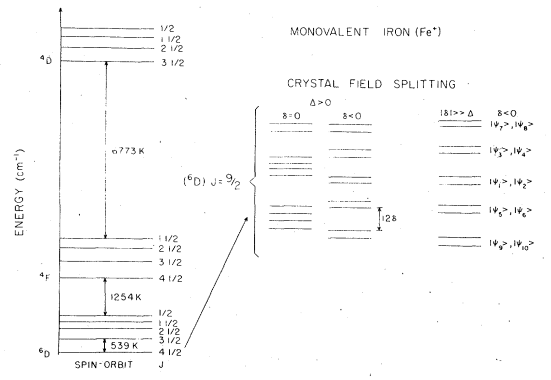

FIG. 8. Fe^+ free ion level splitting and ground state ^6D. The crystal field splitting are shown for ^6D level in a cubic (Δ) and axial (δ) crystal fields.

plicity, the crystal field due to the iodine ions is represented by an axial-field component and it is assumed, as is usual for atoms and ions isolated in a rare-gas solid, that the spin-orbit interaction is stronger than the crystal field. The crystal-field Hamiltonian for this case will be given by[14]

$$H_{CF} = \Delta[35J_z^4 - 30J(J+1)J_z^2 - 6J(J+1) + 3J^2(J+1)^2 + 25J_z^2 + \tfrac{5}{2}(J_+^4 + J_-^4)] + \delta[3J_z^2 - J(J+1)], \quad (1)$$

where Δ is a measure of the strength of the cubic field and δ of the axial field. Figure 8 shows the ionic-level splittings for the free ion and for the ion in the presence of cubic and axial field, where the distance and positions between the Kramers doublets depend on the sign and relative strength of the cubic and axial fields.

Table I lists all the eigenfunctions for the different Kramers doublets of Fig. 8. To evaluate the QS we use the operator equivalent method[15]

$$\langle Im, Jm | H_Q | Im, Jm \rangle = -[3e^2Q/2I(2I-1)](J\|\alpha\|J)\rangle \times \langle r^{-3}\rangle_{3d^{\frac{3}{2}}} (m^2 - \tfrac{1}{3}I(I+1)(J_z^2 - \tfrac{1}{3}J(J+1)), \quad (2)$$

where Q is the quadrupole moment of the nucleus, I is the nuclear spin, and J the angular momentum of the free ion. The conversion factor $(J\|\alpha\|J) = -\frac{1}{63}$. The quadrupole splitting is given by

TABLE I. First column gives the eigenfunctions for the ground state of monovalent iron ($^6D, J = \frac{9}{2}$). Second and third columns give the values for the quadrupole splitting and hyperfine magnetic field, respectively.

Eigenfunctions	QS (mm/sec)	Effective internal field ($H_x = H_y$)
$\psi_1 = \frac{\sqrt{3}}{2\sqrt{2}}\left\|\frac{9}{2}\frac{9}{2}\right\rangle + \frac{\sqrt{7}}{2\sqrt{3}}\left\|\frac{9}{2}\frac{1}{2}\right\rangle + \frac{1}{2\sqrt{6}}\left\|\frac{9}{2}-\frac{7}{2}\right\rangle$	0	H_z = 1350 kOe
$\psi_2 = \frac{\sqrt{3}}{2\sqrt{2}}\left\|\frac{9}{2}-\frac{9}{2}\right\rangle + \frac{\sqrt{7}}{2\sqrt{3}}\left\|\frac{9}{2}-\frac{1}{2}\right\rangle + \frac{1}{2\sqrt{6}}\left\|\frac{9}{2}\frac{7}{2}\right\rangle$		H_x = 2700 kOe
$\psi_3 = \left\|\frac{9}{2}-\frac{5}{2}\right\rangle$	0.6–0.7	H_z = 1840 kOe
$\psi_4 = -\left\|\frac{9}{2}\frac{5}{2}\right\rangle$		H_x = 0
$\psi_5 = -\frac{\sqrt{3}}{4}\left\|\frac{9}{2}\frac{9}{2}\right\rangle + \frac{\sqrt{14}}{4\sqrt{3}}\left\|\frac{9}{2}\frac{1}{2}\right\rangle - \frac{5}{4\sqrt{3}}\left\|\frac{9}{2}-\frac{7}{2}\right\rangle$	0.6–0.7	H_z = 613 kOe
$\psi_6 = \frac{\sqrt{3}}{4}\left\|\frac{9}{2}-\frac{9}{2}\right\rangle\frac{\sqrt{14}}{4\sqrt{3}}\left\|\frac{9}{2}-\frac{1}{2}\right\rangle + \frac{5}{4\sqrt{3}}\left\|\frac{9}{2}\frac{7}{2}\right\rangle$		H_x = 1226 kOe
$\psi_7 = \left\|\frac{9}{2}\frac{3}{2}\right\rangle$	−1.9–2.2	H_z = 1104 kOe
$\psi_8 = -\left\|\frac{9}{2}-\frac{3}{2}\right\rangle$		H_x = 0
$\psi_9 = -\frac{\sqrt{7}}{4}\left\|\frac{9}{2}\frac{9}{2}\right\rangle + \frac{1}{2\sqrt{2}}\left\|\frac{9}{2}\frac{1}{2}\right\rangle + \frac{\sqrt{7}}{4}\left\|\frac{9}{2}\frac{7}{2}\right\rangle$	1.9–2.2	H_z = 368 kOe
$\psi_{10} = \frac{\sqrt{7}}{4}\left\|\frac{9}{2}-\frac{9}{2}\right\rangle - \frac{1}{2\sqrt{2}}\left\|\frac{9}{2}-\frac{1}{2}\right\rangle - \frac{\sqrt{7}}{4}\left\|\frac{9}{2}\frac{7}{2}\right\rangle$		H_x = 736 kOe

$$\Delta E_Q = \tfrac{1}{42} e^2 Q \langle r^{-3} \rangle_{3d} (1-R) \langle J_z^2 - \tfrac{1}{3} J(J-1) \rangle_T , \quad (3)$$

where $\langle J_z^2 - \frac{1}{3} J(J+1) \rangle_T$ means the thermal average over all the different levels. In order to evaluate the QS we need to know the value of $\langle r^{-3} \rangle_{3d}$ for the monovalent iron in the $3d^6 4s^1 (^6D)$ configuration. The value of $\langle r^{-3} \rangle_{3d}$ was calculated using the unrestricted Hartree-Fock approximation and is given in Table II. The quadrupole moment for the first excited state of ^{57}Fe is taken as that given by Ingalls,[16] $Q = 0.21b$. In the absence of an accurate value for the antishielding factor R for Fe^+ we assume that of free Fe^{2+}, $(1-R = 0.7)$. The only possible set of eigenfunctions listed in Table I consistent with the observed QS are $\psi_{9,10}$ or $\psi_{7,8}$; both give the same magnitude for the QS but are opposite in sign. We will show that the high-magnetic-field measurement gives unequivocal evidence that the doublet $\psi_{9,10}$ is the ground state. This result will be seen to be consistent with the case of Fig. 8, where $|\delta| > \Delta$, $\delta < 0$.

A measure of the strength of the crystal-field splitting can be obtained from the temperature dependence of the QS. From the temperature dependence of the QS we obtained a crystal-field splitting between the ground state and the next Kramers doublet equal to 15 K. The overall splitting of all the Kramers doublets in Fig. 8 will be then around 44 K. While these values give only an approximate measure of the strength of the crystal field, due to the uncertainties in $(1-R)\langle r^{-3} \rangle_{3d}$ and Q (approximately 20%), we can conclude that the crystal-field splitting is much weaker than the spin-orbit splitting, as has been observed for other matrix-isolated species in rare gases.

B. Magnetic hyperfine interactions

One expects the internal field for the free monovalent iron to be larger than for neutral iron monomers, due to the presence of an uncompensated $4s$ electron. The $4s$ electron can be coupled to the d shell in two ways, either as $^5d\uparrow d\downarrow 4s\downarrow$ (^4D), or $d^5\uparrow d\downarrow 4s\uparrow$ (^6D). For the free-monovalent iron the ground state is known to be ^6D (Fig. 8). The next possible electronic configuration $3d^7$ has to be disregarded because the observed IS is well outside the expected value for the $3d^7$ ion.[7]

The hyperfine magnetic interaction for the free ion is given by

$$\begin{aligned} H_{mfs} &= a_J \vec{I} \cdot \vec{J} , \\ a_J &= r_J a_l + c \\ a_l &= R_\infty \alpha a_0^3 [(m_e)/M_p] \left\langle \frac{1}{r^3} \right\rangle_{3d} g(I) , \end{aligned} \quad (4)$$

where a_J is the magnetic dipole hyperfine interaction constant. r_J can be evaluated from Ref. 17, c is the s electron's contribution, R_∞ is the Rydberg constant, α is the fine-structure constant, a_0 is

TABLE II. Results of SPHF calculations for the core polarization H_s and orbital and dipolar contribution a_l to the magnetic hyperfine field for the ^6D and ^4D configurations of Fe^+. $\rho(0)$ is the total electron density at the nucleus.

Fe^+ electronic configuration	Shell	$4\pi[\lvert\psi_{ns\uparrow}(0)\rvert^2 - \lvert\psi_{ns\downarrow}(0)\rvert^2]$	$\langle 1/r^3 \rangle$	a_l (Mc/sec)
$3d^5\uparrow 3d\downarrow 4s\downarrow (^4D)$	$1s^2$	−2.35		
	$2s^2$	−34.37		
	$3s^2$	+14.14		
	$4s$	−47.28		
$\rho(0) = \sum_i \lvert\psi_{ni}(0)\rvert^2 = 11\,905.913$ a.u.		−69.86	4.5536	
$\chi = \frac{4\pi}{2s} \sum_n [\lvert\psi_{ns\uparrow}(0)\rvert^2 - \lvert\psi_{ns\downarrow}(0)\rvert^2]$				
$= -23.29$ a.u./unpaired spin				78.4
$H_s = -2.94 \times 10^6$ Oe				
$3d^5\uparrow 3d\downarrow 4s\uparrow (^6D)$	$1s^2$	0.78		
	$2s^2$	−29.78		
	$3s^2$	21.52		
	$4s$	+57.22		
$\rho(0) = 11\,906.875$ a.u.		49.74	4.6909	
$\chi = 9.95$ a.u./unpaired spin				80.8
$H_s = 2.09 \times 10^6$ Oe				

the Bohr hydrogen radius, m_e/M_p is the ratio of the electron mass to the proton mass, and $g(I)$ is the nuclear g factor.

In order to interpret the experimental results in terms of the various contributions to the magnetic hyperfine interaction, we have performed *ab initio* calculations of the terms $3d^6 4s^1(^6D)$ and $3d^6 4s^1(^4D)$ in monovalent iron. For both terms, we have chosen the Hund's-rule state for the d electrons; namely, $3d\uparrow^5 3d\downarrow^1(^5D)$, where the arrows refer to the direction of electron spin. For the ^6D term, the $4s$ electron has its spin aligned with the five d electrons in the half-closed shell (spin-up); for the ^4D term, the $4s$ electron has its spin aligned with the single spin-down d electron.

Since the hyperfine interaction has magnetic dipole, orbital, and contact contributions, including s-electron core polarization, we have used the spin-polarized Hartree-Fock (SPHF) method, which we now summarize.

In the usual restricted Hartree-Fock (RHF), model, the many-electron wave function is chosen to be an antisymmetric product of one-electron orbitals, each of which is assumed to be a product of a space eigenfunction (factored into the product of a spherical harmonic Y and a radial function R) and a spin eigenfunction,

$$\psi n_l m_l m_s = [R_{nl}(r) Y_{l,m_l}(\theta, \phi)] \chi(m_s) . \tag{5}$$

In the RHF theory, the radial function is independent of both the m_s spin and of the m_l orbital momentum projections. While this form of the orbital introduces no restriction for closed-shell systems, this is not the case when one or more shell is only partially filled. Thus, as is well known,[18] since they predict the same density of spin-up and spin-down core electrons in the region of the nucleus, RHF calculations give zero contribution to the hyperfine interaction for closed inner-shell atoms, even for ions which contain open valence shells. To introduce the contribution of these inner-shell electrons, one may remove the restrictions on the radial function R_{nl} and allow it to depend on the projection m_s of the spin, and thus obtain the so called *spin-polarized* Hartree-Fock method (SPHF).

A further step is to allow a dependence of R_{nl} on the projection m_l of the orbital momentum and thus obtain the more sophisticated *spin-plus-orbit-polarized* Hartree-Fock method (SOPHF) in which each electron has a different radial function: relaxing this restriction would have negligible effect in this work; we have therefore remained within the framework of the SPHF model.

In Table II, we present the results of SPHF calculations for the terms ^6D and ^4D. In addition to listing spin densities for each of the s shells, we have calculated values of core-polarization field per unpaired spin in a.u. (χ), as well as total core-polarization field in Oe ($H_c = 4.21 \times 10^4\ 2S \times \chi$). We have also listed total electronic-charge densities at the nucleus, $\rho(0)$, and values of $\langle 1/r^3 \rangle_{3d}$, necessary to obtain orbital and dipolar contributions, as indicated in Eq. (4) above. Note that these values of $\langle 1/r^3 \rangle_{3d}$ are for the $3d\downarrow$ electron only: the five $3d\uparrow$ electrons constitute a half-closed shell, and therefore make no contribution to orbital and dipolar fields. We have neglected any difference in the expectation values of $\langle 1/r^3 \rangle_{3d}$ for the dipolar and orbital terms. A slight difference in the electron densities at the nucleus for the two configurations can be observed in Table II. Using the value of a_l and c as given in Table II, a_J or $H_J(a_J$ or $H_J(a_J \vec{J} \cdot \vec{I} = \mu_N g \vec{H}_J \cdot \vec{I})$ can be calculated. For the ^6D configuration ($J = \frac{9}{2}$) $H_J = 3313$ kOe is obtained. The orbital and dipolar parts give a contribution equal to 1223 kOe. The s-electron contribution is 2090 kOe. Consequently, the expected internal field for the free ion should be very large.

The first striking result of the applied field experiment is the presence in Fig. 7, of a smaller hyperfine magnetic splitting at the ^{57}Fe nucleus than expected from the free-ion results. We will show in what follows that this observed magnetic splitting can be explained by crystal-field effects. The Fe^+ ion is in a crystalline matrix and its ^6D levels will be split by the combined effect of the total crystal field produced by the neighboring xenon atoms and the iodine ions. If one assumes, as is generally the case in a rare-gas matrix, that $H_{so} \gg H_{Zeeman} \gg H_{hf}$, then the evaluation of the expectation value of H_J becomes simple. Due to the fast relaxation time of the electronic magnetic moments compared to the Larmor nuclear precession time, one can define a thermal average for H_J. We will further assume, based upon the temperature dependence of the QS, that at 4.5 K only the ground-state Kramers doublet is populated. For this case it is convenient to express the hyperfine term in the spin Hamiltonian form

$$H_{hf} = \sum_i A_i S_i \cdot I_i , \quad i = x, y, z , \tag{6}$$

where $S = \frac{1}{2}$

$$\begin{aligned} A_{x,y} &= 2a_J \langle \psi + | J_{x,y} | \psi - \rangle , \\ A_z &= 2a_J \langle \psi + | J_z | \psi + \rangle , \end{aligned} \tag{7}$$

for axial symmetry $A_x = A_y$.

It is seen that the hyperfine tensor A is proportional to the g tensor of the doublet. We have neglected in the above relations any mixing of higher ionic J states. In the presence of an external magnetic field the Hamiltonian for the ground-state

doublet is given by

$$H=\sum_i A_i\vec{S}_i\cdot\vec{I}_i-g\mu_B\vec{S}\cdot\vec{H}_{ex}-g_I\mu_N\vec{I}\cdot\vec{H}_{ex}+\vec{H}_Q. \quad (8)$$

The Zeeman term for the ion will remove all degeneracies. Since $H_{\text{Zeeman}}>H_{\text{hf}}$ for each state $|\psi\rangle$, the magnetic hyperfine term can be written as

$$H_{\text{hf}}=g_I\mu_N\vec{H}_{\text{eff}}\cdot\vec{I} \quad (9)$$

The hyperfine interaction splits the nuclear levels in the same way as an external field of magnitude $|H_{\text{eff}}|$. The effective field H_{eff} at the nucleus measured by the Mössbauer spectrum is the sum of the external and internal fields,

$$H_{\text{eff}}=\vec{H}_{\text{ext}}+\vec{H}_N,$$

where

$$\vec{H}_N=\vec{H}_N^0\langle S\rangle/S. \quad (10)$$

The saturation value $H_N^0=AS/g_I\mu_N$ of the internal field is the hyperfine field value that we will compare with the theoretical calculation in Table I. H_{eff} is a function of the crystalline-field parameters, of the magnetic field, and of the direction of the magnetic field relative to the local crystalline-field axes. The hyperfine interaction is diagonalized along an internal direction that need not be parallel to the external-field direction. For relatively small magnetization the internal field will be parallel to the external field. For this case the calculation of the Mössbauer spectrum from the Hamiltonian of Eq. (8) is straightforward.

If the internal magnetic field is not collinear with the external field we will have two independent angles between the EFG principal axis (only the axial field case will be analyzed) and the internal field, and between the internal field and the γ-ray direction. We have selected the γ-ray direction as the quantization axis and consequently we have to average over the two angles. From the analysis of the experimental data we have found that the low-field approximation is more appropriate. One of the major difficulties in our calculation is the distribution of EFG. We will introduce the distribution in the EFG as producing only a broadening of the Mössbauer lines. In the following we will present the results of our calculations using the approach of Collins and Travis.[19] The presence of an asymmetry parameter η, different from zero will only affect the relative intensities of the lines and not the overall splitting. The introduction of the asymmetry parameter will only improve the fit to the spectrum shape.

There are various possibilities for the ground-state doublet depending on the sign and strength of the cubic and axial components of the crystal field. But the Mössbauer spectrum has to be fit both for the magnitude of the QS and the internal field. Only one Kramers doublet from Fig. 8 and Table I gives the correct fit to both hyperfine interactions, namely, $|\psi_9\rangle$ and $|\psi_{10}\rangle$. From this fit we obtained for the internal magnetic field components $H_z=350\pm10$ kOe (theory 368 kOe) and $H_x=700\pm10$ kOe (theory 736 kOe). There is a difference of about 5% between the expected values from Table I and those found experimentally. The sign of the EFG principal axis is positive ($e^2qQ>0$).

V. CONCLUSIONS

This excellent agreement between theory and experiment is striking especially in view of the simplicity of the model used. Although our original purpose was to identify the charge state of the iron ion, the analysis given above, taken together with the free-ion spin-polarized Hartree-Fock calculations, has allowed us to go much further than expected and by obtaining a detailed description of the behavior of the monovalent iron in the rare-gas matrix, to identify the Fe^+ as being in the $3d^6\,4s(^6D)$ state, and to show which Kramers doublet is involved.

---

*Supported by the NSF (DMR Grant Nos. 76-11113, 76-81719, 76-23329.)

†Abteilung Physik und Astronomie, Ruhr-Universitat, Bochum, D-4630 (BRD).

[1]T. K. McNab, H. Micklitz, and P. H. Barrett, Phys. Rev. B 4, 3787 (1971).

[2]H. Micklitz and P. H. Barrett, Phys. Rev. B 5, 1704 (1972).

[3]P. A. Montano, P. H. Barrett, and H. Micklitz, *Mössbauer Effect Methodology*, edited by Irwin J. Gruverman and Carl W. Seidel (Plenum, New York, 1976), Vol. 10, p. 245.

[4]D. M. Mann and H. P. Broida, J. Chem. Phys. 55, 84 (1971).

[5]H. Micklitz and P. H. Barrett, Phys. Rev. B 4, 3045 (1971).

[6]Paul H. Kasai, Phys. Rev. Lett. 21, 67 (1968).

[7]H. Micklitz and P. H. Barrett, Phys. Rev. Lett. 28, 1547 (1972).

[8]H. Micklitz and F. J. Litterst, Phys. Rev. Lett. 33, 480 (1974).

[9]P. A. Montano, P. H. Barrett, and Z. Shanfield, Solid State Commun. 15, 1675 (1974).

[10]P. A. Montano, P. H. Barrett, and Z. Shanfield, J. Chem. Phys. 64, 2896 (1975).

[11]P. H. Barrett and P. A. Montano, J. Chem. Soc. Fara-

day Trans. II 73, 378 (1977).
[12]T. K. McNab, D. H. W. Carstens, D. M. Gruen, and R. L. McBeth, Chem. Phys. Lett. 13, 600 (1972).
[13]F. J. Litterst, G. M. Kalvius, and A. J. F. Boyle, AIP Conf. Proc. 18, 616 (1973).
[14]A. Abragam and B. Bleaney, *Electron Paramagnetic Resonance of Transition Ions* (Clarendon, Oxford, 1970).
[15]H. Eicher, Z. Phys. 169, 178 (1962).
[16]R. Ingalls, Phys. Rev. B 188, 1045 (1969).
[17]R. E. Trees, Phys. Rev. 92, 308 (1953).
[18]R. E. Watson and A. J. Freeman, Phys. Rev. 123, 2027 (1961).
[19]R. L. Collins and J. C. Travis, in *Mössbauer Effect Methodology*, edited by I. J. Gruverman (Plenum, New York, 1967), Vol. 3.